

T -odd quark pair production and decay at $\gamma\gamma$ collider in the littlest Higgs model with T parity in next-to-leading order QCD

Liu Wen,¹ Ma Wen-Gan,¹ Guo Lei,² Chen Liang-Wen,¹ Chen Chang,¹ and Zhang Ren-You¹

¹Department of Modern Physics, University of Science and Technology of China (USTC),
Hefei, Anhui 230026, P.R.China

²Department of Physics, Chongqing University, Chongqing 401331, P.R. China

Abstract

We calculate the complete next-to-leading order (NLO) QCD corrections to the T -odd mirror quark pair ($q-\bar{q} = u-\bar{u}, c-\bar{c}, d-\bar{d}, s-\bar{s}$) production in the littlest Higgs model with T -parity (LHT) at a high energy $\gamma\gamma$ collider. We present the dependence of the leading order (LO) and NLO QCD corrected cross sections on the colliding energy \sqrt{s} . Our calculation includes the subsequent full weak decays of the final T -odd mirror quarks by adopting the narrow width approximation and the exclusive 2-jet event selection criterion. We provide the LO and QCD NLO kinematic distributions of final particles. We find that the NLO QCD correction is phase space dependent and modifies the LO cross section evidently. The K -factor increases noticeably when \sqrt{s} approaches the threshold of the on-shell q -pair production. We conclude that it is possible to separate the signature of the T -odd quark pair production from possible Standard Model background by taking proper kinematic cut.

PACS: 12.38.Bx, 13.85.Lg, 13.85.Hd

Keywords: Littlest Higgs model with T parity, T -odd quark pair production, photon-photon collider

I. Introduction

Recently the discovery of a new particle that resembles the Standard Model (SM) Higgs boson was announced simultaneously by the CMS and ATLAS collaborations at CERN Large Hadron Collider [1, 2]. This amazing discovery is an important milestone of physics and has given an impetus to the study of the electroweak symmetry breaking (EWSB) mechanism. Subsequent analyses are still in process to determine the traits of the new boson.

Although the SM has made immense success in explaining fundamental particle interactions, there are still crucial questions, such as the famous hierarchy problem and the search for new physics. In order to solve the hierarchy problem in the SM, several models have been proposed. Among them the little Higgs mechanism [3–5] is one of the elegant candidates. The littlest Higgs model (LHM) is the most economical realization of the little Higgs mechanism and a phenomenologically viable model. In the LHM, a scalar triplet Φ , a new vector-like quark T and a set of new heavy gauge bosons (W_H , A_H , Z_H) are introduced. However, the mixture of the SM gauge bosons and the heavy new gauge bosons leads to stringent constraints on the LHM. Motivated by these constraints, a new discrete symmetry, denoted as “ T -parity”, is introduced [6–10]. In the littlest Higgs model with T -parity (LHT), all the SM particles are T -even while all new particles are T -odd except T_+ . As a result of the T -parity conservation, the mixture between the SM gauge bosons and the heavy new gauge bosons is prohibited and no triplet vacuum expectation value (VEV) is generated. Consequently, the strong electroweak constraints on the model are significantly relaxed. In the LHT, a neutral, colorless and weakly interacting stable particle A_H is predicted and can be a good candidate for dark matter [8–12], which has gained a lot of attention.

The CERN Large Hadron Collider can directly produce very massive new particles and will extend the possibilities of finding new physics effects, but it cannot easily provide precision measurements due to the typical characteristic of hadron machine. Whereas, a TeV scale linear collider with extremely high luminosity and clean experimental environment, can provide complementary information on these properties with precision measurements that would complete the results from hadron collider experiment. A most popularly proposed linear collider with energies at TeV scale and extremely high luminosity is the Compact Linear Collider (CLIC) [13, 14]. In addition to e^+e^- collision, linear collider provides a suitable platform running in $\gamma\gamma$ and γe collision modes at energies and luminosities comparable with those in e^+e^- collision mode through the laser backscattering procedure [15, 16].

The LHT phenomenology of the T -odd quarks has been extensively studied. The effects of the T -odd fermions in high energy scattering processes were explored in Ref. [17]. Recently, the T -odd quark signals at the LHC and

ILC were studied at the QCD NLO in Refs. [18–21], and the QCD NLO correction to the T -odd gauge boson associated with a T -odd quark production at the LHC was reported in Ref. [22, 23].

We investigate the q_+ -pair production up to the QCD NLO in the LHT at the future high energy $\gamma\gamma$ collider, including subsequent decays of the final T -odd quarks in this paper. The content is organized as follows: In Sec. II, we briefly review the related LHT theory, and provide the corresponding mass spectrum. In Sec. III, the calculation strategy is presented. In Sec. IV, numerical analysis and discussion are provided. The last section is devoted to the summary.

II. Related LHT theory and mass spectrum

The LHT is a nonlinear σ -model based on the $SU(5)/SO(5)$ global symmetry breaking at some high energy scale f , leading to 14 massless Nambu-Goldstone bosons described by the “ Π ” matrix as

$$\Pi = \begin{pmatrix} -\frac{\omega^0}{2} - \frac{\eta}{\sqrt{20}} & -\frac{\omega^+}{\sqrt{2}} & -i\frac{\pi^+}{\sqrt{2}} & -i\phi^{++} & -i\frac{\phi^+}{\sqrt{2}} \\ -\frac{\omega^-}{\sqrt{2}} & \frac{\omega^0}{2} - \frac{\eta}{\sqrt{20}} & \frac{v+h+i\pi^0}{2} & -i\frac{\phi^+}{\sqrt{2}} & \frac{-i\phi^0+\phi^P}{\sqrt{2}} \\ i\frac{\pi^-}{\sqrt{2}} & \frac{v+h-i\pi^0}{2} & \sqrt{4/5}\eta & -i\frac{\pi^+}{\sqrt{2}} & \frac{v+h+i\pi^0}{2} \\ i\phi^{--} & i\frac{\phi^-}{\sqrt{2}} & i\frac{\pi^-}{\sqrt{2}} & -\frac{\omega^0}{2} - \frac{\eta}{\sqrt{20}} & -\frac{\omega^-}{\sqrt{2}} \\ i\frac{\phi^-}{\sqrt{2}} & \frac{i\phi^0+\phi^P}{\sqrt{2}} & \frac{v+h-i\pi^0}{2} & -\frac{\omega^+}{\sqrt{2}} & \frac{\omega^0}{2} - \frac{\eta}{\sqrt{20}} \end{pmatrix}. \quad (2.1)$$

Among the 14 Nambu-Goldstone bosons, η , ω^0 and ω^\pm are the Goldstone bosons associated with the spontaneous gauge symmetry breaking

$$[SU(2) \otimes U(1)]_1 \otimes [SU(2) \otimes U(1)]_2 \rightarrow SU(2)_L \otimes U(1)_Y, \quad (2.2)$$

and are eaten by the heavy gauge bosons A_H , Z_H and W_H^\pm , respectively. The other 10 Nambu-Goldstone bosons constitute two $SU(2)_L$ multiplets: (1) T -even SM Higgs doublet $H \sim (\pi^+, h + v, \pi^0)$, where h is the SM Higgs boson, $v \simeq 246$ GeV the Higgs VEV, and $\pi^{0,\pm}$ are the Goldstone bosons eaten by the SM gauge bosons, and (2) T -odd scalar triplet $\Phi \sim (\phi^{++}, \phi^+, \phi^0, \phi^P)$.

The $[SU(2) \otimes U(1)]_1 \otimes [SU(2) \otimes U(1)]_2$ gauge fields B_i and W_i^a ($i = 1, 2$, $a = 1, 2, 3$) transform under T parity as

$$B_1 \longleftrightarrow B_2, \quad W_1^a \longleftrightarrow W_2^a. \quad (2.3)$$

The heavy gauge bosons A_H , Z_H and W_H^\pm are the T -odd eigenstates of the $[SU(2) \otimes U(1)]_1 \otimes [SU(2) \otimes U(1)]_2$

gauge fields, and therefore can be expressed as

$$\begin{pmatrix} A_H \\ Z_H \end{pmatrix} = \begin{pmatrix} \cos \theta_H & -\sin \theta_H \\ \sin \theta_H & \cos \theta_H \end{pmatrix} \begin{pmatrix} \frac{1}{\sqrt{2}} & -\frac{1}{\sqrt{2}} & 0 & 0 \\ 0 & 0 & \frac{1}{\sqrt{2}} & -\frac{1}{\sqrt{2}} \end{pmatrix} \begin{pmatrix} B_1 \\ B_2 \\ W_1^3 \\ W_2^3 \end{pmatrix},$$

$$W_H^\pm = \frac{(W_1^1 - W_2^1) \mp i(W_1^2 - W_2^2)}{2}. \quad (2.4)$$

At $\mathcal{O}(v^2/f^2)$, the masses of the T -odd heavy gauge bosons are given by

$$m_{A_H} = \frac{1}{\sqrt{5}} g' f \left(1 - \frac{5}{8} \frac{v^2}{f^2} \right), \quad m_{Z_H} = m_{W_H} = g f \left(1 - \frac{1}{8} \frac{v^2}{f^2} \right), \quad (2.5)$$

and the mixing angle θ_H has the form as

$$\sin \theta_H = \frac{5gg'}{4(5g^2 - g'^2)} \frac{v^2}{f^2}, \quad (2.6)$$

where g and g' are the $SU(2)_L$ and $U(1)_Y$ gauge couplings, respectively.

A consistent implementation of T parity in the quark sector requires the introduction of the T -odd mirror quarks for the SM quarks. For each quark flavor, we introduce the following two incomplete left-handed $SU(5)$ multiplets and a right-handed $SO(5)$ multiplet:

$$\Psi_1 = \begin{pmatrix} \psi_1 \\ 0 \\ 0 \end{pmatrix}, \quad \Psi_2 = \begin{pmatrix} 0 \\ 0 \\ \psi_2 \end{pmatrix}, \quad \Psi_{HR} = \begin{pmatrix} \tilde{\psi}_{HR} \\ \chi_{HR} \\ \psi_{HR} \end{pmatrix}, \quad (2.7)$$

with

$$\psi_A = -\tau^2 q_A = -\tau^2 \begin{pmatrix} u_A \\ d_A \end{pmatrix}, \quad (A = 1, 2, HR), \quad (2.8)$$

where τ^2 is the second Pauli matrix. The transformations for these fields under $SU(5)$ tell us that q_1 , q_2 and q_{HR} are all $SU(2)_L$ doublets. Under T parity, Ψ_1 , Ψ_2 and Ψ_{HR} transform as

$$\Psi_1 \longrightarrow -\Sigma_0 \Psi_2, \quad \Psi_2 \longrightarrow -\Sigma_0 \Psi_1, \quad \Psi_{HR} \longrightarrow -\Psi_{HR}, \quad (2.9)$$

where Σ_0 is a 5×5 symmetric tensor defined as

$$\Sigma_0 = \begin{pmatrix} & & 1_{2 \times 2} \\ & 1 & \\ 1_{2 \times 2} & & \end{pmatrix}. \quad (2.10)$$

Thus, the T -parity eigenstates of the $SU(2)_L$ quark doublets q_A ($A = 1, 2, HR$) are

$$\begin{aligned} q_{SM} &= \frac{q_1 - q_2}{\sqrt{2}}, & (T - \text{even}), \\ q_{HL} &= \frac{q_1 + q_2}{\sqrt{2}}, & q_{HR}, & (T - \text{odd}). \end{aligned} \quad (2.11)$$

q_{SM} is the left-handed $SU(2)_L$ SM quark doublet, while q_{HL} the left-handed $SU(2)_L$ mirror quark doublet. The right-handed $SU(2)_L$ mirror quark doublet is given by q_{HR} .

The T -odd mirror quarks acquire masses via the following Lagrangian:

$$\mathcal{L}_{\text{mirror}} = - \sum_{i,j=1}^3 \kappa f \delta_{ij} \left(\bar{\Psi}_2^i \xi + \bar{\Psi}_1^i \Sigma_0 \Omega \xi^\dagger \Omega \right) \Psi_{HR}^j + \text{h.c.}, \quad (2.12)$$

where $\Omega = \text{diag}(1, 1, -1, 1, 1)$, $\xi = e^{i\Pi/f}$, $i, j = 1, \dots, 3$ are flavor indices, and κ is the mass coefficient of T -odd mirror quarks. Assuming a flavor independent coupling, the masses of the T -odd up- and down-type quarks at the $\mathcal{O}(v^2/f^2)$ are given by

$$m_{u_{i-}} = \sqrt{2} \kappa f \left(1 - \frac{1}{8} \frac{v^2}{f^2} \right), \quad m_{d_{i-}} = \sqrt{2} \kappa f, \quad (2.13)$$

where $u_{i-} = u_-, c_-, t_-$ and $d_{i-} = d_-, s_-, b_-$ with i running from 1 to 3.

In order to cancel the large quadratic divergent correction to the Higgs boson mass induced by the top quark, a T -even top-quark partner T_+ is introduced. The implementation of T parity then requires also a T -odd partner T_- . The Yukawa interaction for the top sector is given by

$$\begin{aligned} \mathcal{L}_{\text{top}} = & -\frac{1}{2\sqrt{2}} \lambda_1 f \epsilon_{ijk} \epsilon_{xy} \left[(\bar{Q}_1)_i (\Sigma)_{jx} (\Sigma)_{ky} - (\bar{Q}_2 \Sigma_0)_i (\tilde{\Sigma})_{jx} (\tilde{\Sigma})_{ky} \right] u_R \\ & - \lambda_2 f (\bar{U}_{L1} U_{R1} + \bar{U}_{L2} U_{R2}) + \text{h.c.}, \end{aligned} \quad (2.14)$$

where $\Sigma = e^{2i\Pi/f} \Sigma_0$, and $\tilde{\Sigma} = \Sigma_0 \Omega \Sigma^\dagger \Omega \Sigma_0$ is the image of Σ under T parity. The $SU(5)$ multiplets Q_1 and Q_2 are defined as

$$Q_1 = \begin{pmatrix} \psi_1 \\ U_{L1} \\ 0 \end{pmatrix}, \quad Q_2 = \begin{pmatrix} 0 \\ U_{L2} \\ \psi_2 \end{pmatrix}, \quad (2.15)$$

which obey the same transformation laws under T parity and $SU(5)$ as do Ψ_1 and Ψ_2 . U_{L1} and U_{L2} are left-handed $SU(2)_L$ singlets. U_{R1} , U_{R2} and u_R are all right-handed $SU(2)_L$ singlets, and transform under T parity as

$$U_{R1} \leftrightarrow -U_{R2}, \quad U_{R2} \leftrightarrow -U_{R1}, \quad u_R \leftrightarrow u_R. \quad (2.16)$$

Then we obtain the following T -parity eigenstates

$$U_{L\pm} = \frac{U_{L1} \mp U_{L2}}{\sqrt{2}}, \quad U_{R\pm} = \frac{U_{R1} \mp U_{R2}}{\sqrt{2}}, \quad u_R, \quad (2.17)$$

in addition to those in (2.11). From the top Yukawa Lagrangian (2.14), we can get the mass eigenstates of the top sector. The T -odd eigenstates U_{L-} and U_{R-} do not mix with the T -odd mirror quarks, while the T -even

eigenstates U_{L+} and U_{R+} mix with u_{SM} and u_R , respectively, so that the mass eigenstates of the top quark t and its heavy partners T_{\pm} are given by

$$\begin{aligned} \begin{pmatrix} t_L \\ (T_+)_L \end{pmatrix} &= \begin{pmatrix} \cos \theta_L & -\sin \theta_L \\ \sin \theta_L & \cos \theta_L \end{pmatrix} \begin{pmatrix} u_{SM} \\ U_{L+} \end{pmatrix}, & (T_-)_L &= U_{L-}, \\ \begin{pmatrix} t_R \\ (T_+)_R \end{pmatrix} &= \begin{pmatrix} \cos \theta_R & -\sin \theta_R \\ \sin \theta_R & \cos \theta_R \end{pmatrix} \begin{pmatrix} u_R \\ U_{R+} \end{pmatrix}, & (T_-)_R &= U_{R-}. \end{aligned} \quad (2.18)$$

The masses of T_+ and T_- can be expressed as

$$\begin{aligned} m_{T_+} &= \frac{f}{v} \frac{m_t}{\sqrt{x_L(1-x_L)}} \left[1 + \frac{v^2}{f^2} \left(\frac{1}{3} - x_L(1-x_L) \right) \right], \\ m_{T_-} &= \frac{f}{v} \frac{m_t}{\sqrt{x_L}} \left[1 + \frac{v^2}{f^2} \left(\frac{1}{3} - \frac{1}{2}x_L(1-x_L) \right) \right], \end{aligned} \quad (2.19)$$

where

$$m_t = v \sqrt{x_L(1-x_L)(\lambda_1^2 + \lambda_2^2)} \left[1 + \frac{v^2}{f^2} \left(-\frac{1}{3} + \frac{1}{2}x_L(1-x_L) \right) \right], \quad x_L = \lambda_1^2/(\lambda_1^2 + \lambda_2^2), \quad (2.20)$$

and $\lambda_{1,2}$ are the Yukawa coupling constants of top sector.

III. Calculations

The T -odd mirror quark pair production at a photon-photon collider, denoted as $\gamma(p_1) + \gamma(p_2) \rightarrow q_-(p_3) + \bar{q}_-(p_4)$, is a pure electromagnetic process at the leading order. The tree-level Feynman diagrams are depicted in Fig.1. The LO differential cross section for this process is simply given by

$$d\sigma_{LO}(\gamma\gamma \rightarrow q_-\bar{q}_-) = \frac{1}{4} \frac{(2\pi)^4 N_c}{4|\vec{p}_1|\sqrt{s}} \sum_{\text{spin}} |\mathcal{M}_t + \mathcal{M}_u|^2 d\Phi_2, \quad (3.1)$$

where $N_c = 3$, \sqrt{s} is the center-of-mass energy of the photon-photon collision, the summation is taken over the spins of the initial and final states, $d\Phi_2$ is the two-body phase-space element defined as

$$d\Phi_2 = \delta^{(4)}(p_1 + p_2 - p_3 - p_4) \prod_{i=3}^4 \frac{d^3\vec{p}_i}{(2\pi)^3 2E_i}, \quad (3.2)$$

and \mathcal{M}_t , \mathcal{M}_u are the amplitudes for the t - and u -channel Feynman diagrams, respectively, expressed as

$$\mathcal{M}_t = -iQ_{q_-}^2 \bar{u}(p_3) \not{\epsilon}(p_1) \frac{1}{\not{p}_3 - \not{p}_1 - m_{q_-}} \not{\epsilon}(p_2) v(p_4), \quad \mathcal{M}_u = \mathcal{M}_t \Big|_{p_1 \leftrightarrow p_2}. \quad (3.3)$$

Since the third generation of T -odd mirror quarks, b_- and t_- , can be identified in experiment, we only consider the T -odd mirror quark pair production of the first two generations in $\gamma\gamma$ collision. Both the total and differential

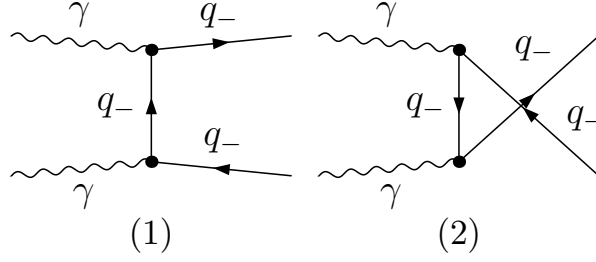


Figure 1: The tree-level Feynman diagrams for the $\gamma\gamma \rightarrow q_- \bar{q}_-$ process.

cross sections for the $\gamma\gamma \rightarrow q_- \bar{q}_-$ process presented in this paper are summed over the $u_- \bar{u}_-$, $d_- \bar{d}_-$, $c_- \bar{c}_-$ and $s_- \bar{s}_-$ production processes.

The NLO QCD corrections to the $\gamma\gamma \rightarrow q_- \bar{q}_-$ process include virtual loop and real emission corrections, which contain ultraviolet (UV) and infrared (IR) singularities. We adopt the dimensional scheme for renormalization, in which the dimensions of both the spinor and space-time manifolds are extended to $D = 4 - 2\epsilon$, to regularize these divergences. Since the physical observables are UV- and IR-finite, all the UV and IR divergences should be canceled. The virtual loop correction contains both the UV and IR singularities. In the on-mass-shell renormalization scheme, the T -odd mirror quark wave function and mass renormalization constants are expressed as

$$\begin{aligned} \delta Z_{q_-}^{L,R} &= -\frac{\alpha_s(\mu_r)}{3\pi} \left[\Delta_{UV} + 2\Delta_{IR} + 4 + 3 \ln \left(\frac{\mu_r^2}{m_{q_-}^2} \right) \right], \\ \frac{\delta m_{q_-}}{m_{q_-}} &= -\frac{\alpha_s(\mu_r)}{3\pi} \left\{ 3 \left[\Delta_{UV} + \ln \left(\frac{\mu_r^2}{m_{q_-}^2} \right) \right] + 4 \right\}, \end{aligned} \quad (3.4)$$

where $\Delta_{UV} = \frac{1}{\epsilon_{UV}} - \gamma_E + \ln(4\pi)$ and $\Delta_{IR} = \frac{1}{\epsilon_{IR}} - \gamma_E + \ln(4\pi)$ are the UV and IR regulators, respectively. The UV divergence associated with these renormalization constants can cancel exactly those arising from the loop integrals. Then the virtual correction is UV-finite after performing the renormalization procedure.

Although the renormalized virtual correction is UV-finite, it still contains the IR-soft singularity. According to the Kinoshita-Lee-Nauenberg theorem [24, 25], the IR-soft singularity of the renormalized virtual correction can be canceled by that of the real gluon emission correction. We denote the real gluon emission process for the T -odd mirror quark pair production at a $\gamma\gamma$ collider as $\gamma(p_1) + \gamma(p_2) \rightarrow q_-(p_3) + \bar{q}_-(p_4) + g(p_5)$. In our NLO calculations for the $\gamma\gamma \rightarrow q_- \bar{q}_-$ process there exists QCD soft IR-singularity, but no QCD collinear IR-singularity. In order to manipulate the IR-soft singularity, we employ the phase-space slicing method proposed by B. W. Harris and J. F. Owens [26]. A soft cutoff δ_s is introduced to separate the phase space of the $\gamma\gamma \rightarrow q_- \bar{q}_- g$ process into two regions, the soft gluon region ($E_5 \leq \frac{1}{2}\delta_s\sqrt{s}$) and the hard gluon region ($E_5 > \frac{1}{2}\delta_s\sqrt{s}$). The IR-soft singularity is located at

the soft gluon region, while the phase-space integration over the hard gluon region is finite and can be evaluated in the four dimensions by using the Monte Carlo technique.

Finally, the total cross section for the T -odd mirror quark pair production at a photon-photon collider at the QCD NLO can be expressed as

$$\sigma_{NLO} = \sigma_{LO} + \Delta\sigma_{NLO} = \sigma_{LO} + \left[\sigma^V + \sigma_S^R \right] + \sigma_H^R, \quad (3.5)$$

where σ^V , σ_S^R and σ_H^R are the renormalized virtual correction, real soft gluon emission correction and real hard gluon emission correction, respectively. As mentioned above, both $\left[\sigma^V + \sigma_S^R \right]$ and σ_H^R are finite, and therefore can be calculated numerically.

The T -odd mirror quarks are unstable particles, thus we should consider their decay channels in studying the kinematic distributions of the final products of the T -odd mirror quark pair production. The main decay modes of the T -odd mirror quark q_- are $q_- \rightarrow W_H q'$, $q_- \rightarrow Z_H q$ and $q_- \rightarrow A_H q$, i.e., $\Gamma_{q_-}^{\text{tot}} \simeq \Gamma(q_- \rightarrow W_H q') + \Gamma(q_- \rightarrow Z_H q) + \Gamma(q_- \rightarrow A_H q)$, with the LO decay widths expressed as [27]

$$\begin{aligned} \Gamma_{LO}(q_{i-} \rightarrow A_H q_j) &= \frac{|(V_{Hq})_{ij}|^2}{32\pi} \left(\frac{g}{2} \sin \theta_H + I_{qj} \frac{g'}{5} \cos \theta_H \right)^2 \frac{m_{q_{i-}}^3}{m_{A_H}^2} \left(1 - \frac{m_{A_H}^2}{m_{q_{i-}}^2} \right)^2 \left(1 + \frac{2m_{A_H}^2}{m_{q_{i-}}^2} \right), \\ \Gamma_{LO}(q_{i-} \rightarrow Z_H q_j) &= \frac{|(V_{Hq})_{ij}|^2}{32\pi} \left(\frac{g}{2} \cos \theta_H - I_{qj} \frac{g'}{5} \sin \theta_H \right)^2 \frac{m_{q_{i-}}^3}{m_{Z_H}^2} \left(1 - \frac{m_{Z_H}^2}{m_{q_{i-}}^2} \right)^2 \left(1 + \frac{2m_{Z_H}^2}{m_{q_{i-}}^2} \right), \\ \Gamma_{LO}(q_{i-} \rightarrow W_H q'_j) &= \frac{|(V_{Hq'})_{ij}|^2}{64\pi} g^2 \frac{m_{q_{i-}}^3}{m_{A_H}^2} \left(1 - \frac{m_{A_H}^2}{m_{q_{i-}}^2} \right)^2 \left(1 + \frac{2m_{A_H}^2}{m_{q_{i-}}^2} \right), \quad (i, j = 1, 2), \end{aligned} \quad (3.6)$$

where the the first two generation quarks are taken to be massless and

$$q'_j = \begin{cases} d, s, & (\text{for } q_{i-} = u_-, c_-) \\ u, c, & (\text{for } q_{i-} = d_-, s_-) \end{cases}, \quad I_{qj} = \begin{cases} +\frac{1}{2}, & (q_j = u, c) \\ -\frac{1}{2}, & (q_j = d, s), \end{cases} \quad (3.7)$$

and V_{Hu} , V_{Hd} are CKM-like unitary mixing matrices satisfying $V_{Hu}^\dagger V_{Hd} = V_{CKM}$. We neglect the mixing between the first two generations and the third generation. At the QCD NLO, the partial decay width for the $q_{i-} \rightarrow V_H q'_j$ decay mode has the form as

$$\Gamma_{NLO}(q_{i-} \rightarrow V_H q'_j) = \Gamma_{LO}(q_{i-} \rightarrow V_H q'_j) \times \left[1 + \frac{2\alpha_s}{3\pi} \left(\frac{2\pi^2}{3} - \frac{5}{2} \right) + \mathcal{O} \left(\frac{\alpha_s}{\pi} \frac{m_{V_H}^2}{m_{q_{i-}}^2} \right) \right]. \quad (3.8)$$

We evaluate the terms of $\mathcal{O} \left(\frac{\alpha_s}{\pi} \frac{m_{V_H}^2}{m_{q_{i-}}^2} \right)$ ($V_H = A_H, Z_H, W_H$ and $q_- = u_-, d_-, c_-, s_-$), and find that their contributions to the branch ratios are less than 0.01% in the parameter space adopted in this work, and therefore can be neglected.

f (GeV)	m_{u_-} (GeV)	m_{d_-} (GeV)	$m_{W_H} \approx m_{Z_H}$ (GeV)	m_{A_H} (GeV)	m_{T_+} (GeV)	m_{T_-} (GeV)
700	974.7	989.9	442.1	99.2	996.6	715.5
800	1118.0	1131.4	507.1	115.6	1136.3	812.9
900	1260.9	1272.8	571.9	131.8	1276.2	910.8
1000	1403.5	1414.2	636.6	147.8	1416.4	1009.1

Table 1: The masses of relevant heavy new particles in the LHT for some typical values of f with $\kappa = 1$ and $x_L = 1/2$. (x_L is only used in calculating the masses of T_+ and T_- .)

We use the FeynArts-3.4 package developed by us to generate Feynman diagrams and their corresponding amplitudes for the $\gamma\gamma \rightarrow q_-\bar{q}_-$ process in the LHT at both the LO and QCD NLO, and employ the FormCalc-5.4 program for algebraic manipulation. The IR singularities of loop integrals are isolated analytically by using our developed-in-house programs, and the IR-finite parts are calculated numerically based on the LoopTools-2.4 package. The analytical expressions for the IR-singular parts of loop integrals and the formulas for evaluating the IR-finite N -point ($N \leq 4$) integrals are given in Refs. [28–30], respectively.

IV. Numerical results and discussions

In this section we provide and discuss the numerical results for the T -odd mirror quark pair production at a $\gamma\gamma$ collider in the LHT up to the QCD NLO. The SM electroweak input parameters for our calculations are taken as: $\alpha_{\text{ew}}^{-1} = 137.036$, $m_W = 80.385$ GeV and $m_Z = 91.1876$ GeV [31]. The u -, d -, c - and s -quarks are treated as massless particles, and the CKM matrix is set to be the unit matrix, i.e., $V_{CKM} = I$. Considering the latest results from the 8 TeV run at the LHC, the constraints from Higgs couplings are by now competing with electroweak precision tests and both exclude f up to 694 GeV or 560 GeV depending on the implementation of the down-type Yukawa sector [32]. In our numerical calculations, we constrain the global symmetry breaking scale of the LHT in the range of $f \geq 700$ GeV. The T -odd mirror quark mass coefficient κ is fixed to be 1 in default unless stated otherwise, and the two CKM-like matrices are taken as $V_{Hu} = I$ and $V_{Hd} = V_{CKM}$. In the NLO QCD calculations for the $\gamma\gamma \rightarrow q_-\bar{q}_-$ process, we set the QCD renormalization scale being $\mu = \mu_r = m_{q_-}$. In Table 1 we present the masses of heavy particles in the LHT for some typical values of the LHT global symmetry breaking scale f .

Since the summation of all the QCD NLO contributions should be numerically finite, we verify the correctness of our calculation by means of confirming the cancellations of the UV and IR divergences. To isolate the soft IR divergences, we introduce an arbitrary cutoff δ_s to separate the phase space. The total NLO QCD corrected cross

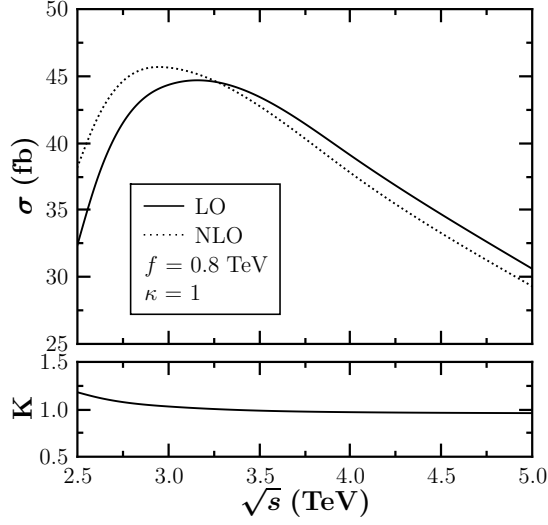


Figure 2: The LO, NLO QCD corrected cross sections and the corresponding K -factor for $\gamma\gamma \rightarrow q_-\bar{q}_-$ as functions of the colliding energy \sqrt{s} with $f = 800$ GeV.

section (σ_{NLO}) for the $\gamma\gamma \rightarrow q_-\bar{q}_-$ process is obtained by summing up the two-body and three-body contribution parts ($\sigma_{LO} + \Delta\sigma^{(2)} = \sigma_{LO} + \sigma^V + \sigma_S^R$ and $\Delta\sigma^{(3)} = \sigma_H^R$). The σ_{NLO} should be independent of δ_s [26]. We check the independence of the NLO QCD corrected integrated cross section on the cutoff δ_s within the statistical errors by varying the cutoff δ_s in the range of $[1 \times 10^{-6}, 1 \times 10^{-4}]$ with $\sqrt{s} = 3$ TeV, $\kappa = 1$ and $f = 700$ GeV. This is also an indirect verification for the correctness of our calculation. In further numerical calculations, we fix $\delta_s = 1 \times 10^{-4}$.

To study the dependence of cross sections on the colliding energy \sqrt{s} , we plot the LO, NLO QCD corrected cross sections (σ_{LO} , σ_{NLO}) and the corresponding K -factor defined as $K = \frac{\sigma_{NLO}}{\sigma_{LO}}$ for the $\gamma\gamma \rightarrow q_-\bar{q}_-$ process as the functions of \sqrt{s} with $f = 800$ GeV in Fig.2. Both the LO and NLO QCD corrected cross sections obviously go up with the increment of colliding energy in the range near the $q_-\bar{q}_-$ production threshold, while decrease rapidly when \sqrt{s} goes up beyond 3200 GeV as shown in the upper plot of Fig.2. And we can see from the lower plot of Fig.2, the K -factor has a relative large value in the vicinity of the $q_-\bar{q}_-$ threshold.

The LO and NLO QCD corrected integrated cross sections at a $\sqrt{s} = 3$ TeV photon-photon collider and the corresponding K -factors as functions of the global symmetry breaking scale f are plotted in Fig.3, separately. Since the masses of final q_- and \bar{q}_- become heavier with the increment of f and make the phase space getting smaller, the LO and NLO QCD corrected total cross sections for the $\gamma\gamma \rightarrow q_-\bar{q}_-$ process would decrease with the increment of f as demonstrated in Fig.3. The K -factor in the lower plot of Fig.3 gradually increases with the increment of f due to the fact that the threshold value ($2m_{q_-}$) moves towards the colliding energy with the increment of f . From

f (GeV)	σ_{LO} (fb)	σ_{NLO} (fb)	K
700	57.3691(1)	56.708(3)	0.99
800	44.34106(9)	45.6365(9)	1.03
900	30.65976(9)	33.7591(4)	1.10
1000	15.92042(1)	20.48004(6)	1.29

Table 2: The LO, NLO QCD corrected cross sections and the corresponding K -factor for the $\gamma\gamma \rightarrow q-\bar{q}$ process for some typical values of f at a $\sqrt{s} = 3$ TeV photon-photon collider.

Fig.3 we read out some numerical results for the $\gamma\gamma \rightarrow q-\bar{q}$ process at a $\sqrt{s} = 3$ TeV photon-photon collider for some typical values of f , and listed them in Table 2.

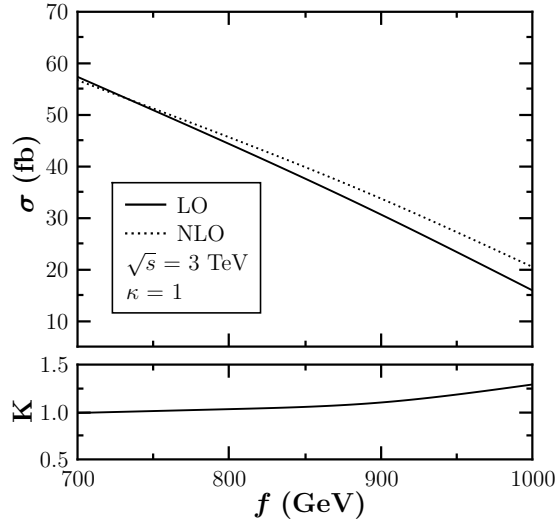


Figure 3: The LO, NLO QCD corrected integrated cross sections and the corresponding K -factor for the $\gamma\gamma \rightarrow q-\bar{q}$ process as functions of the global symmetry breaking scale f at a $\sqrt{s} = 3$ TeV photon-photon collider.

The LO, NLO QCD corrected integrated cross sections and the corresponding K -factors versus the LHT T -odd quark mass coefficient κ at the $\sqrt{s} = 3$ TeV photon-photon collider with $f = 0.8, 0.9$ and 1.0 TeV are plotted in Figs.4(a-c), separately. As shown in these figures both the LO and NLO QCD corrected cross sections decrease with the increment of κ , while the K -factor increases with the increase of κ . That is because the threshold value approaches the colliding energy when κ goes up. One can read out from the figures that for $f = 0.8$ TeV the corresponding K -factor varies from 0.95 to 1.51 with κ going up from 0.6 to 1.3, for $f = 0.9$ TeV the K -factor increases from 0.96 to 1.25 with κ running from 0.6 to 1.1, while for $f = 1.0$ TeV the K -factor goes up from 0.97 to 1.29 with κ increasing from 0.6 to 1.0.

In the following, we investigate the kinematic distributions of final particles after the on-shell T -odd mirror

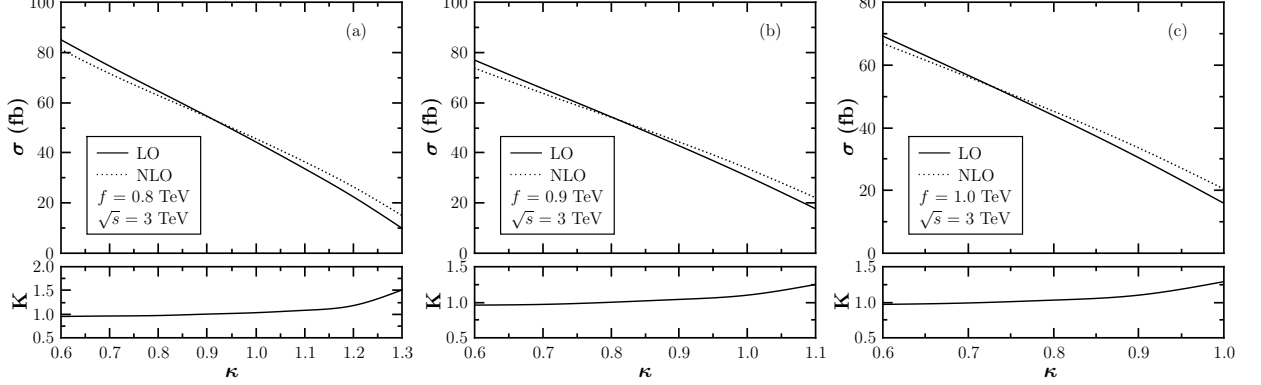


Figure 4: The LO, NLO QCD corrected cross sections and the corresponding K -factors for the $\gamma\gamma \rightarrow q-\bar{q}$ process as functions of the T -odd mirror quark mass coefficient κ at the $\sqrt{s} = 3$ TeV photon-photon collider. (a) $f = 0.8$ TeV. (b) $f = 0.9$ TeV. (c) $f = 1.0$ TeV.

quark decays ($q_-[\bar{q}_-] \rightarrow A_H q[\bar{q}]$), adopting the narrow width approximation. The $q_-[\bar{q}_-]$ decay products involve a $q[\bar{q}]$ -jet and missing energy of the lightest neutral stable particle A_H . Its SM background should be mainly from the $\gamma\gamma \rightarrow q\bar{q}Z \rightarrow q\bar{q}\nu\bar{\nu}$ process, where $q\bar{q} = u\bar{u}, c\bar{c}, d\bar{d}, s\bar{s}$. According to Eq.(3.8) one can obtain the $q_- \rightarrow A_H q$ decay branch ratio up to the QCD NLO. After the decays of the T -odd mirror quarks, we may encounter the event with several jets in the analyses. We adopt the Cambridge/Aachen (C/A) jet algorithm [33, 34] provided by the **Fastjet** package [35] with the distance parameter $R = 0.4$ to merge the proto-jets. The recombined i -th and j -th jets gain its four-momentum by $p_\mu^{ij} = p_\mu^i + p_\mu^j$. After the jet merging procedure, theoretically we may meet three kind of events, i.e., 1-jet, 2-jet and 3-jet events. In the following analyses, we collect the “2-jet” events by adopting the exclusive 2-jet event selection criterion to collect the signal and background events:

- (I) For theoretical 2-jets events, we accept the event with both two jets satisfying the condition of $p_T^j > 20$ GeV.
- (II) For theoretical 3-jets events, we accept the event with only two hardest jets satisfying the constraints of $p_T^j > 20$ GeV and the remained jet satisfying $p_T^j < 20$ GeV.

In Fig.5 we plot the LO and NLO QCD corrected distributions of the final missing transverse momentum (p_T^{miss}) for the $\gamma\gamma \rightarrow q-\bar{q} \rightarrow 2A_H + 2jets$ process at a $\sqrt{s} = 3$ TeV photon-photon collider, and the corresponding K -factor defined as $K(p_T^{miss}) \equiv \frac{d\sigma_{NLO}/dp_T^{miss}}{d\sigma_{LO}/dp_T^{miss}}$. There we take $f = 700$ GeV and get $m_{A_H} = 99.2$ GeV. Both the LO and NLO differential cross sections reach their maxima in the vicinity of $p_T^{miss} \sim 580$ GeV, and the corresponding K -factor varies from 0.81 to 0.84 when p_T^{miss} goes up from 0 to 1400 GeV as displayed in the figure.

In a “2-jet” event, we name the jets with the largest energy and the second largest energy as the leading jet and

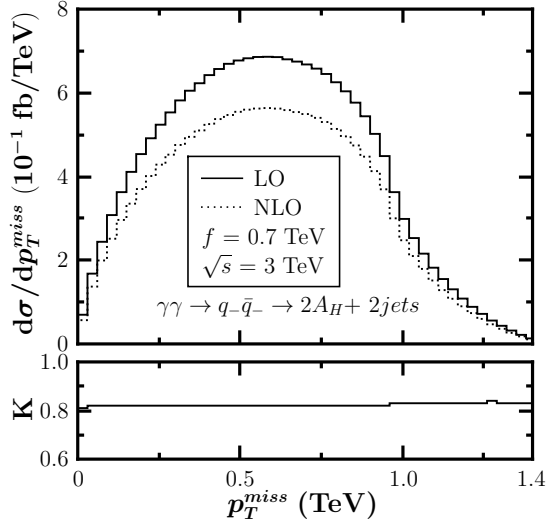


Figure 5: The LO, NLO QCD corrected distributions of the missing transverse momentum (p_T^{miss}), and the corresponding K -factor for the $\gamma\gamma \rightarrow q-\bar{q} \rightarrow 2A_H + 2jets$ process at a $\sqrt{s} = 3$ TeV photon-photon collider.

next-to-leading jet, respectively. In Fig.6(a) we present the LO and NLO QCD corrected transverse momentum distributions of the leading jet at the $\sqrt{s} = 3$ TeV photon-photon collider and the corresponding K -factor defined as $\left[K(p_T^{L-jet}) \equiv \frac{d\sigma_{NLO}/dp_T^{L-jet}}{d\sigma_{LO}/dp_T^{L-jet}} \right]$. Here we take $f = 700$ GeV, and then get $m_{A_H} = 99.2$ GeV. The peaks for the LO and QCD NLO curves are located in the vicinity of $p_T^{L-jet} \sim 600$ GeV, and the K -factor varies in the range of $[0.80, 0.83]$ when p_T^{L-jet} goes up from 100 GeV to 1300 GeV as shown in the figure.

In Fig.6(b) we plot the LO and NLO QCD corrected distributions of the rapidity separation of the final leading-jet and next-to-leading jet ($|\Delta y| \equiv |y_{L-jet} - y_{NL-jet}|$), and the corresponding K -factor ($K(|\Delta y|) \equiv \frac{d\sigma_{NLO}/d|\Delta y|}{d\sigma_{LO}/d|\Delta y|}$). We see that most of the $\gamma\gamma \rightarrow q-\bar{q} \rightarrow 2A_H + 2jets$ events are concentrated in the low $|\Delta y|$ region and the K -factor varies between 0.80 and 0.83 with $|\Delta y|$ in the range of $[0, 4]$. All the distributions in Fig.5 and Figs.6(a,b) show that the K -factor is not very sensitive to the kinematic variables, such as the transverse momentum, jet rapidity separation etc. But it would be necessary to calculate the complete NLO QCD corrections to get reliable kinematic distributions in the precision measurement.

For the $\gamma\gamma \rightarrow q-\bar{q} \rightarrow 2A_H + 2jets$ signal process at a photon-photon collider, the main SM background comes from the $\gamma\gamma \rightarrow q\bar{q}Z \rightarrow q\bar{q}\nu\bar{\nu}$ process with two resolved jets. We define parameter H_T as $H_T = \sum_i |\vec{p}_T(i)|$ which is the scalar sum of the transverse momenta of all the final jets for both signal and background events. By adopting the exclusive 2-jet event selection scheme mentioned above, we present the normalized total QCD corrected H_T distributions for the signal, and the LO distribution for its SM background in the upper panel of Fig.7. There the

distributions are normalized by the corresponding total cross sections. We can see that the SM background events tend to be concentrated in the low H_T region with a peak in the vicinity of $H_T \sim 220$ GeV and then its event number declines rapidly. While the total QCD corrected H_T distribution for the q_{-} -pair production signature has flatter peak in the vicinity of $H_T \sim 1800$ GeV and descends slowly as illustrated in Fig.7. That indicates if we take proper lower limit on H_T parameter, the background from the $\gamma\gamma \rightarrow q\bar{q}Z \rightarrow q\bar{q}\nu\bar{\nu}$ process can be significantly suppressed. In the lower figure of Fig.7 we show the corresponding K -factors of the H_T distribution for the signal process, where we can see that the K -factor for the signature H_T distribution varies in the range of $0.80 - 0.88$ with the increment of H_T from 120 GeV to 3 TeV.

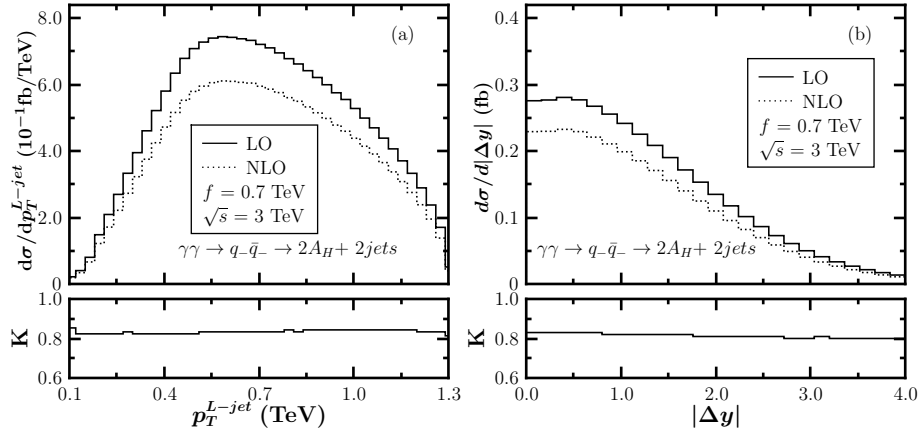


Figure 6: (a) The LO, NLO QCD corrected transverse momentum distributions of the leading jet and the corresponding K -factor for the $\gamma\gamma \rightarrow q_{-}\bar{q}_{-} \rightarrow 2A_H + 2jets$ process at the $\sqrt{s} = 3$ TeV photon-photon collider. (b) The LO, NLO QCD corrected distributions and the corresponding K -factor as functions of the rapidity separation of the final leading jet and next-to-leading jet $|\Delta y| \equiv |y_{L-jet} - y_{NL-jet}|$ at the $\sqrt{s} = 3$ TeV photon-photon collider.

V. Summary

In this paper we present the precision calculations of the T -odd mirror quark pair production including subsequent weak decays at a photon-photon collider up to the QCD NLO in the littlest Higgs model with T -parity. The relationship between the LO, NLO QCD corrected integrated cross sections and the colliding energy \sqrt{s} is investigated, and the LO and NLO QCD corrected kinematic distributions of final decay products are presented. We find that the K -factor is dependent on the phase space region, and increases significantly when the colliding energy approaches the q_{-} -pair production threshold. We see that the K -factor for the integrated cross section varies in the ranges of $0.99 \sim 1.29$ with f in the range of $f \in [700, 1000]$ GeV at a $\sqrt{s} = 3$ TeV photon-photon collider. We conclude that NLO QCD corrections make relevant quantum impact on the $\gamma\gamma \rightarrow q_{-}\bar{q}_{-} \rightarrow 2A_H + 2jets$ processes, and should

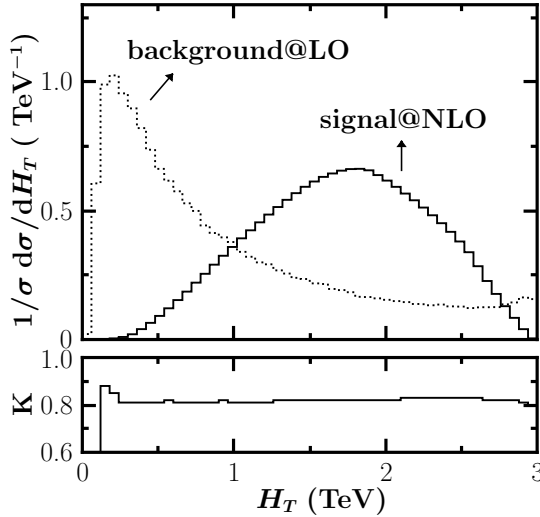


Figure 7: The normalized H_T distributions for the signal process $\gamma\gamma \rightarrow q-\bar{q} \rightarrow 2A_H + 2jets$ up to the QCD NLO with $f = 700$ GeV and the SM background process $\gamma\gamma \rightarrow q\bar{q}Z \rightarrow q\bar{q}\nu\bar{\nu}$ at the LO at a 3 TeV photon-photon collider. The corresponding QCD K -factors for the signal process are plotted in the lower panel.

be included in any reliable analysis. We compare the H_T distributions for the T -odd quark pair production signal and the main SM background, and conclude that they are remarkably different, and $\gamma\gamma \rightarrow q-\bar{q} \rightarrow 2A_H + 2jets$ signal events can be discriminated from the possible $\gamma\gamma \rightarrow q\bar{q}Z \rightarrow q\bar{q}\nu\bar{\nu}$ background by taking proper cut on the H_T .

VI. Acknowledgments

This work was supported in part by the National Natural Science Foundation of China (Grants. No.11275190, No.11375008, No.11375171).

References

- [1] S. Chatrchyan *et al.* [CMS Collaboration], Phys. Lett. **B716** (2012) 30.
- [2] G. Aad *et al.* [ATLAS Collaboration], Phys. Lett. **B716** (2012) 1.
- [3] N. Arkani-Hamed, A.G. Cohen, and H. Georgi, Phys. Lett. **B513** (2001) 232.
- [4] M. Schmaltz and D. Tucker-Smith, Annu. Rev. Nucl. Part. Sci. **55** (2005) 229.
- [5] M. Perelstein, Prog. Part. Nucl. Phys. **58** (2007) 247, and references therein.
- [6] H.-C. Cheng, I. Low, JHEP **09** (2003) 051.

- [7] H.-C. Cheng, I. Low, JHEP **08** (2004) 061.
- [8] I. Low, JHEP **10** (2004) 067.
- [9] J. Hubisz and P. Meade, Phys. Rev. **D71** (2005) 035016.
- [10] J. Hubisz, P. Meade, A. Noble and M. Perelstein, JHEP **01** (2006) 135.
- [11] R. Barbieri and A. Strumia, “The ‘LEP paradox’”, arXiv:hep-ph/0007265.
- [12] H.C. Cheng and I. Low, JHEP **09** (2003) 051; **08** (2004) 061.
- [13] H. Braun, *et al.*, CLIC-NOTE-764, [CLIC Study Team Collaboration], CLIC 2008 parameters, <http://www.clic-study.org>.
- [14] H. Abramowicz, *et al.*, “Physics at the CLIC e^+e^- Linear Collider – Input to the Snowmass process 2013”, arXiv:1307.5288.
- [15] I.F. Ginzburg, G.L. Kotkin, S.L. Panfil, V.G. Serbo and V.I. Telnov, Nucl. Instrum. Meth. **219** (1984) 5.
- [16] I.F. Ginzburg, G.L. Kotkin, V.G. Serbo and V.I. Telnov, Nucl. Instrum. Meth. **205** (1983) 47.
- [17] A. Belyaev, C.-R. Chen, K. Tobe and C.-P. Yuan, Phys. Rev. **D74** (2006) 115020.
- [18] D. Choudhury, D.K. Ghosh and S.K. Rai, JHEP **07** (2012) 013.
- [19] D. Choudhury and D.K. Ghosh, JHEP **08** (2007) 084.
- [20] S. Mukhopadhyay, B. Mukhopadhyaya and A. Nyffeler, JHEP **05** (2010) 001.
- [21] A.B. Mahfoudh, L. Guo, W. Liu, W.-G. Ma, R.-Y. Zhang and W.-J. Zhang, Commun. Theor. Phys. **62** (2014) 824.
- [22] R.-Y. Zhang, H. Yan, W.-G. Ma, S.-M. Wang, L. Guo and L. Han, Phys. Rev. **D85** (2012) 015017.
- [23] X.-D. Yang, S.-J. Xiong, W.-G. Ma, R.-Y. Zhang, L. Guo and X.-Z. Li Phys. Rev. **D89** (2014) 014008.
- [24] T. Kinoshita, J. Math. Phys. **3** (1962) 650.
- [25] T.D. Lee and M. Nauenberg, Phys. Rev. **133** (1964) B1549.

- [26] B.W. Harris and J.F. Owens, Phys. Rev. **D65** (2002) 094032.
- [27] S.-M. Du, L. Guo, W. Liu, W.-G. Ma and R.-Y. Zhang, Phys. Rev. **D86** (2012) 054027.
- [28] R.K. Ellis and G. Zanderighi, JHEP **02** (2008) 002.
- [29] G. 't Hooft and M. Veltman, Nucl. Phys. **B153** (1979) 365.
- [30] A. Denner, U. Nierste and R. Scharf, Nucl. Phys. **B367** (1991) 637.
- [31] J. Beringer, *et al.* (Particle Data Group), Phys. Rev. **D86** (2012) 010001.
- [32] J. Reuter, M. Tonini and M. de Vries, JHEP **02** (2014) 053.
- [33] M. Cacciari, G.P. Salam and G. Soyez, JHEP **04** (2008) 063.
- [34] G.P. Salam, Eur. Phys. J. **C67** (2010) 637.
- [35] M. Cacciari, G.P. Salam and G. Soyez, Eur. Phys. J. **C72** (2012) 1896.